Topological Programmability of Isomerizable Polymers

Qionghai Chen,[1,*] Xiuyang Xia,[2,3,*] Wanhui Huang,[1] Liqun Zhang,[1] Ran Ni,[2,†] and Jun Liu[1,‡]
[1]State Key Laboratory of Organic-Inorganic Composites, Beijing University of Chemical Technology, Beijing 100029, People's Republic of China
[2]School of Chemistry, Chemical Engineering and Biotechnology, Nanyang Technological University, 62 Nanyang Drive, Singapore 637459, Singapore
[3]Arnold Sommerfeld Center for Theoretical Physics and Center for NanoScience, Department of Physics, Ludwig-Maximilians-Universität München, Theresienstraße 37, D-80333 München, Germany

(Received 30 October 2023; accepted 20 June 2024; published 24 July 2024)

Topology isomerizable networks (TINs) can be programmed into numerous polymers exhibiting unique and spatially defined (thermo-) mechanical properties. However, capturing the dynamics in topological transformations and revealing the intrinsic mechanisms of mechanical property modulation at the microscopic level is a significant challenge. Here, we use a combination of coarse-grained molecular dynamics simulations and reaction kinetic theory to reveal the impact of dynamic bond exchange reactions on the topology of branched chains. We find that, the grafted units follow a geometric distribution with a converged uniformity, which depends solely on the average grafted units of branched chains. Furthermore, we demonstrate that the topological structure can lead to spontaneous modulation of mechanical properties. The theoretical framework provides a research paradigm for studying the topology and mechanical properties of TINs.

DOI: 10.1103/PhysRevLett.133.048101

While cross-linked thermoset polymers boast remarkable properties, their utility is often hampered by the irreversible nature of covalent bonds. A promising strategy involves integrating dynamic bond exchange reactions (BERs) into their molecular frameworks [1–5], namely, vitrimers, enabling the formation and reformation of dynamic covalent bonds in response to external stimuli [6–11]. This adaptation allows the polymers to topologically rearrange their network without compromising their three-dimensional integrity. Consequently, dynamic covalent polymeric networks demonstrate unique adaptive capabilities not present in traditional covalent networks, including self-healing, reprocessability, thermoresponsive gelling, and permanent shape reconfiguration [12–24].

In conventional vitrimer materials, dynamic covalent bonds facilitate structural modifications through BERs. However, this mechanism does not address the intrinsic topological heterogeneity of these materials, which is characterized by a nonuniform distribution of chain lengths within the polymer network. As a result, the properties of these materials remain nonprogrammable. While it can induce topological heterogeneity by incorporating external molecules, this approach has restricted applicability and is limited to non-cross-linked polymer solutions or melts [25]. Contrarily, topology isomerizable networks (TINs) offer a paradigm shift, allowing for topological transitions within a "fully enclosed" material without external agents [26,27]. This isomerization mechanism typically requires designing materials to initially possess network heterogeneity. For example, TINs with long grafted chains can transform into a brush network upon light activation using a photolatent catalyst. Halting light exposure can lock intermediate topological states, preventing complete uniformity and illustrating the capacity of TINs for programmable material properties through topological control [26].

Despite the execution of experimental studies on topological isomerizable networks, the precise experimental capture of topology presents significant challenges. This difficulty introduces ambiguity concerning the ideal reaction endpoint needed to attain the desired network topology, thereby hindering the establishment of a clear connection between topology and material properties. In this Letter, we seek to close this gap by combining molecular dynamics simulations and reaction kinetics theory. Our research delves into the temporal evolution and equilibrium distribution of branched chain lengths, further investigating how the uniformity of branching impacts mechanical properties.

Model—We consider a coarse-grained system consisting of 100 polymer chains, each comprising 31 backbone beads. As shown in Fig. 1(a), the ends of each polymer backbone (depicted in green) are irreversibly cross-linked by tetrafunctional cross-linker molecules to form rubberlike networks, achieving 99% cross-linkage (see Supplemental

*These authors contributed equally to this letter.
†r.ni@ntu.edu.sg
‡liujun@mail.buct.edu.cn

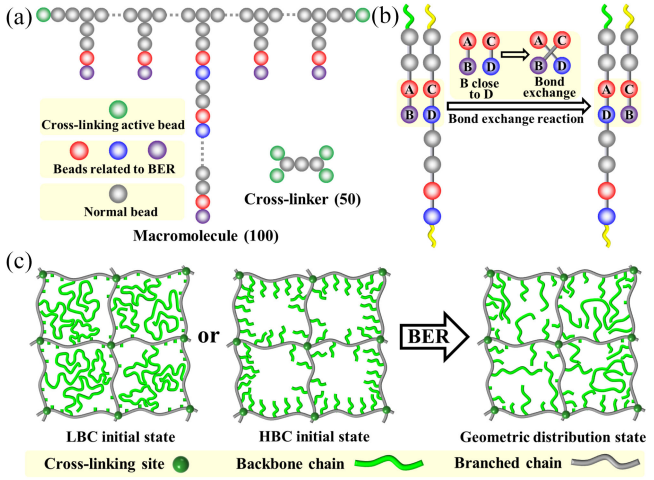

FIG. 1. Coarse-grained model for topology isomerizable networks. Schematic diagrams of (a) polymer and cross-linker models for the long branched chain (LBC) state, (b) bond exchange reaction (BER), and (c) topological changes after BERs starting from the LBC or HBC state.

Material [28]). Distributed uniformly along each polymer backbone are five branched chains, each terminated by an end-type active unit (depicted in purple) to initiate BERs. In the branched chains, every four beads are considered as one repeating unit. As shown in Fig. 1(b), we replicate the BER dynamics described in the topology isomerizable network, where the end-type units attack and exchange bonds with the middle repeated units (depicted in blue) on the branched chains, thereby acquiring the rest length of the attacked branched chains [26]. The red beads can prevent the BERs inconsistent with the experiment (Fig. S1). The BER incorporates an activation energy ΔE_{sw}, aligning with experimental conditions [3,4].

For our simulations, we utilize coarse-grained molecular dynamics (CGMD) with BERs to explore various system topologies, employing the large-scale atomic/molecular massively parallel simulator (LAMMPS) [29]. All nonbonded interactions are modeled using a Lennard-Jones (LJ) potential [30], characterized by the dimensionless LJ units ϵ and σ. The harmonic potential models the bond stretching energy between adjacent beads [31,32]. We simulate BERs using the `fix bond/react` command in LAMMPS [33,34]. Specifically, as shown in Fig. 1(b), if the distance between beads B and D falls below σ, the covalent bonds $A-B$ and $C-D$ break, and two new covalent bonds, $A-D$ and $B-C$, form with a specific probability $p_{\mathrm{sw}} = e^{-\beta\Delta E_{\mathrm{sw}}}$, where $\beta = 1/(k_{\mathrm{B}}T)$ with k_{B} and T as the Boltzmann constant and the temperature of the system, respectively. This process ensures that the total number of covalent bonds in the system remains constant. The simulations commence with all beads arranged in a nonoverlapping configuration within a simulation box, with periodic boundary conditions in three dimensions. We employ the NPT MD simulations to equilibrate the systems with the Nosé-Hoover temperature thermostat and pressure barostat to $T = 1.0$ and $P = 1.0$, respectively. At equilibrium, we observe the total number density $\rho \approx 0.85$, akin to the density of a polymer melt [35]. Detailed simulation information and parameters are available in the Supplemental Material [28] and Refs. [36–42]).

With reference to the polydispersity index of polymer chains [43], we introduce the branched chain uniformity α to quantify the topology of branched chains:

$$\alpha = \langle (l+1)^2 \rangle / \langle l+1 \rangle^2, \tag{1}$$

where l represents the number of middle repeated units on branched chains, and 1 signifies the end repeated unit. $\langle \cdots \rangle$ computes the average over the distribution of the length of branched chains, with the mathematical estimate $\langle l \rangle = s = m/n$, where m represents the number of middle repeated units, and n denotes the number of end repeated units, which also corresponds to the number of branched chains. We examine the system starting from two different initial states: the long branched chain (LBC) state and the homogeneously branched chain (HBC) state. In the LBC state, all middle repeated units of a polymer chain are concentrated in one branched chain, representing the most inhomogeneous initial state with $\alpha = 4.16$. Conversely, the HBC state represents the most homogeneous distribution of branched chain lengths with $\alpha = 1.00$, where each chain consists of s middle repeated units. In our simulations, s was set to 8, except in cases where s was varied as a parameter under discussion. Figure 1(c) demonstrates the change in topology, illustrating that the two initial states can reach the same exponentially distributed state after BERs.

Dynamical analysis of α—We plot the simulation results of the probability of the i-units branched chain at time t, denoted as $P(i,t)$, from both LBC and HBC states with various ΔE_{sw} in Fig. 2(a). With increasing time, the branched chain uniformity α from both states gradually approaches and fluctuates around a constant value. The effect of temperature on the time evolution of α exhibits a similar phenomenon (Fig. S2). Besides, Fig. 2(b) further illustrates the dependence of the constant value on s. These suggest that various states of topological heterogeneity characterized by α can be kinetically trapped by deactivating the BERs. Hence, determining the time when BERs are deactivated to achieve the targeted α is critical. By neglecting the dissociative rings formed by self-attacking reactions and assuming that the diffusion timescale of active beads is far quicker than that of BERs, we write the master equation of the probability of i middle units of branched chains with $0 \le i \le m$:

$$\frac{\mathrm{d}P(i,t)}{K\mathrm{d}t} = \sum_{j=0}^{i-1} [w_{j\to i}^{+} P(j) - w_{i\to j}^{-} P(i)] + \sum_{j=i+1}^{m} [w_{j\to i}^{-} P(j) - w_{i\to j}^{+} P(i)], \tag{2}$$

where the influx of i-units chains can be achieved by two paths: (i) the end of a shorter j-units chain ($j < i$) attacks one middle unit on other chains which are longer than $i - j$; and (ii) the longer j-units chain ($j > i$) is attacked by the end of other chains. The transition probabilities of the two paths are given by $w^{+}_{j\to i} = \sum_{k=i-j}^{m} P(k)/m$ and $w^{-}_{j\to i} = 1/m$, respectively. We note that the superscript $^{+}$ indicates the growth of the chain while $^{-}$ indicates shrinkage. Similarly, two paths are associated with the outflux of i-units chains: (iii) the i-units chain is attacked by the end of other chains and leaves j units with the transition probability $w^{-}_{i\to j} = 1/m$, and (iv) the end of the i-units chain attacks the other chain to form j units with the transition probability $w^{+}_{i\to j} = \sum_{k=j-i}^{m} P(k)/m$.

The BER rate $K = k_0 n e^{-\beta\Delta E_{sw}}$ quantifies the frequency of BERs, with k_0 signifying the pre-exponential factor. To determine k_0, we analyze the normalized bond autocorrelation function $C_{sw}(t) = \overline{\langle N_b(t_0)\cdot N_b(t_0+t)\rangle}$, where $N_b(t_0)$ represents the count of active bonds initially present at time t_0, and $N_b(t_0+t)$ corresponds to the count at a subsequent time t_0+t. The lifetime of the BER τ_{sw} is defined as the time when C_{sw} is decayed to $1/e$, i.e., $C_{sw}(\tau_{sw}) = 1/e$. Figures S3a and S3c show the $C_{sw}(t)$ for different ΔE_{sw} at T systems, and Figs. S3b and S3d show the corresponding τ_{sw}. The Arrhenius equation is found to be fully compatible with the $C_{sw}(t)$ for different ΔE_{sw} at T systems with $\tau_{sw} = \tau_0 e^{\beta\Delta E_{sw}}$. For the system with n grafted sites, the BER rate K can be obtained from the τ_{sw} as $K = n/\tau_{sw} = k_0 n e^{-\beta\Delta E_{sw}}$, where $k_0 = 1/\tau_0$. These results also indicate that lower ΔE_{sw} and higher T result in higher K.

The excellent agreement between theoretical and simulation results at higher ΔE_{sw} validates the accuracy of our theory. This theoretical framework offers a pathway to precisely regulate the level of topological heterogeneity. It achieves this by dictating the deactivation timing of the BERs, thereby enabling the determination of distinct structural configurations. At lower ΔE_{sw}, discrepancies arise between the theoretical and simulation results, predominantly due to the diffusion dynamics of the branched chains. In scenarios where branched chains have inadequate time to diffuse, "ineffective reactions" may ensue, i.e., multiple BERs occur between two dynamic bonds without resulting in structural alterations of the branched chains, as shown in Fig. 2(c). A reduction in $\beta\Delta E_{sw}$ elevates the BER rate, leading to ineffective reactions increasing. Consequently, this discrepancy causes the simulation results to trail behind the theoretical predictions, as shown in Fig. 2(a).

Next, we provide an intuitive theoretical description to analytically derive the equilibrium distribution of the length of branched chains α_E. At the thermodynamic limit $m, n \gg 1$, we examine the detailed balance condition between i- and $(i+1)$-unit branched chains, expressed as $P_E(i)w^{+}_{i\to i+1} = P_E(i+1)w^{-}_{i+1\to i}$. We have $P_E(i+1)/P_E(i) = 1 - P_E(0)$,

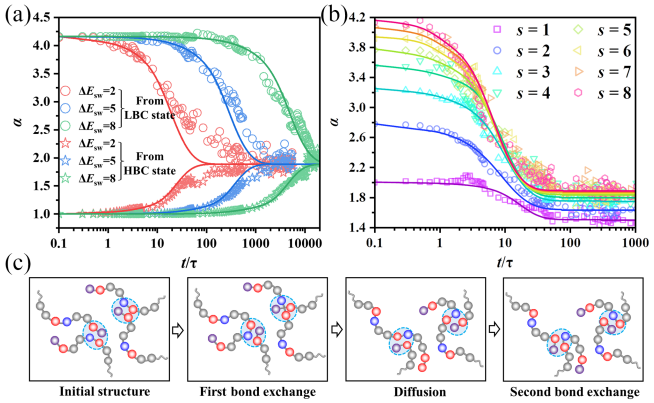

FIG. 2. Dynamical analysis of α. (a) Time evolution of α from initial states of LBC and HBC for various ΔE_{sw} under $s = 8$. (b) Time evolution of α from the LBC initial state for various s under $\Delta E_{sw} = 0$. (c) Schematic diagram of "ineffective reactions." After two rounds of BERs, the length of the branched chains remained unchanged.

indicating that P_E follows a geometric distribution $P_E(i) = P_E(0)[1 - P_E(0)]^i$, with the probability of zero-unit chains given by $P_E(0) = 1/(s+1)$. Remarkably, this analytical solution for the distribution quantitatively agrees with simulation results without any fitting parameters [Fig. 3(a)]. Furthermore, for the systems with the same s, $P_E(i)$ collapse to a master curve regardless of the variations in parameters such as activation energy ΔE_{sw}, temperature T, strength of interbranch interaction ϵ_{bb}, and stiffness of the branched chains k_{branch} (Fig. S4). We note that the mean and the variance of the distribution are given by $\langle l\rangle = s$ and $\langle l^2\rangle = s(s+1)$, respectively. Thus, the equilibrium branched chain uniformity can be expressed as $\alpha_E = 2 - 1/(s+1)$, which also closely corresponds with simulation results across various s systems [Fig. 3(b)]. We ascertain that the maximum α_E at the limit of long branched chains with $\alpha_E(s\to\infty) = 2$. Experimentally, the number of middle units per branched chain significantly exceeds that in the simulation models currently constructed. Therefore, it is inferred that after enduring extensive BERs, the α value converges to 2.

Mechanical properties modulation—To investigate the mechanical properties of different topologies in TINs, we perform uniaxial extension and measure the tension where BERs are inactivated under various α. As shown in Fig. 4(a), we measure the stress under a fixed strain $\varepsilon_T = 5$ at different average branched chain lengths s and starting from HBC and LBC, respectively. We find that as the reaction time evolves, corresponding to the branched uniformity converges to α_E, the mechanical properties characterized by σ_T increase. We select six configurations to display their complete stress-strain curves [Fig. 4(b)], and we find that when the strain is sufficiently large, the mechanical properties of the configurations closer to α_E are better. This implies a spontaneous regulation of the mechanical properties by the topology, i.e., the mechanical properties are optimal near the equilibrium state.

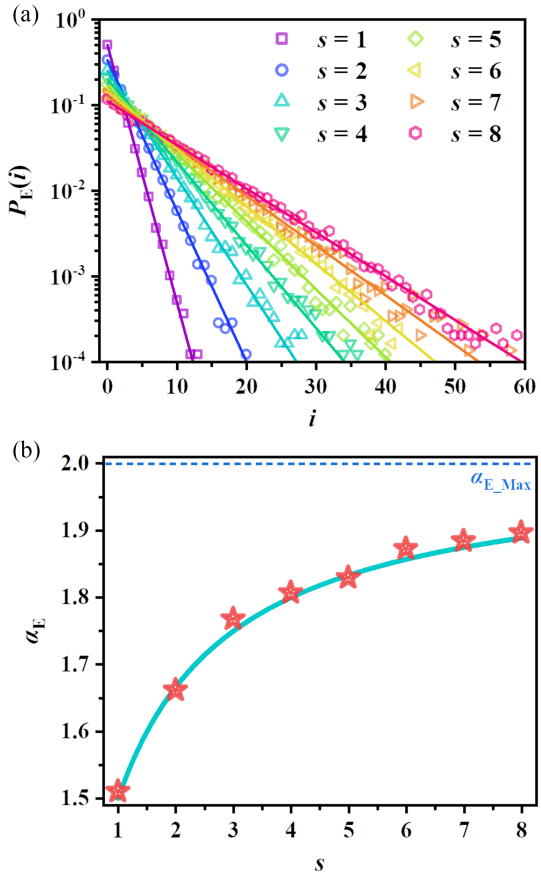

FIG. 3. Equilibrium distributions and uniformity. (a) Middle unit distribution of branched chains at equilibrium $P_E(i)$ for a different average number of middle unit s systems. Solid lines are from theoretical derivation. (b) Branched chain uniformity in equilibrium α_E as a function of s. Solids line is calculated from $\alpha_E = 2 - 1/(s+1)$, while dashed line indicates the maximum value of α_E under the large-s limit with $\alpha_E(s \to \infty) = 2$. In all figures, symbols are obtained from the simulations.

To further understand the spontaneous regulation behavior, we examined the entanglement behavior for the selected configurations with an entanglement degree $\lambda = \sum L_p / \sum L_c$, where $\sum L_p$ and $\sum L_c$ represent the total primitive path lengths [44] and contour lengths of all polymer chains when the polymers are relaxed, respectively, as shown in the inset of Fig. 4(c). We note that higher λ indicates a greater degree of entanglement. As shown in Fig. 4(c), the entanglement degree peaks around the configuration closest to α_E, which indicates that the maximum entanglement is achieved under the geometric distribution of the branched chain length.

The contribution of the entanglement primarily occurs between branched chains, as well as between branched chains and the backbone chains (Fig. S5). Moreover, higher entanglement degrees facilitate polymer chain orientation during stretching (Fig. S6a), enhancing stress contributions from covalent bonds along the stretching direction (manifested as larger bond energy, Fig. S6b). The system with α_E presents the highest molecular chain orientation due to the greatest entanglement degree, which leads to optimal mechanical properties.

Discussion—In conclusion, we used CGMD simulations to study a polymeric system allowing bond-exchange reactions and exhibiting topological isomerization. We investigate the dynamics of branch uniformity, characterized by α, by constructing a reaction kinetic theory. Moreover, the theory effectively guides how to achieve the desired topology experimentally by adjusting the initial configuration and reaction rate. In our models, we determined that α_E depends solely on average branch chain length, which aligns well with simulation results across different system variables. Additionally, contrary to the common belief that branching chain lengths are uniformly distributed at equilibrium [26], our simulation and theoretical results reveal the branched chain lengths at equilibrium follow a geometric distribution. This theoretical framework is applicable to analyze the topology of polymer systems such as star [45] and bottle brush [46] polymers. Besides, we propose a mechanism explaining the influence of topology on mechanical properties. Optimal properties are achieved when α reaches equilibrium, indicating an intelligent regulation of mechanical performance through

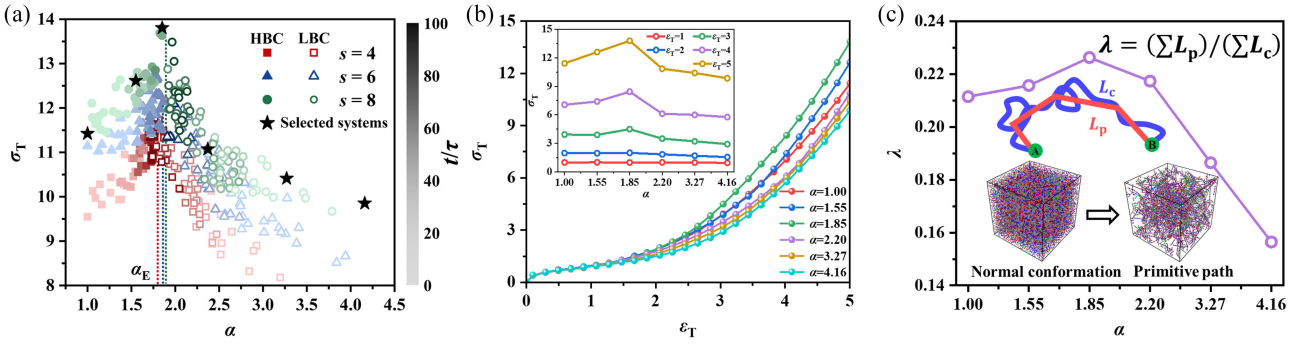

FIG. 4. Mechanical properties modulation. (a) Stresses σ_T at $\epsilon_T = 5$ for 120 different α systems. (b) Stress-strain curves for selected different α marked by the black symbol in (a). The inset shows the stress as a function of α at different strains. (c) Entanglement degree as a function of α. The inset shows a schematic representation of the calculation of entanglement degree λ, as well as a comparison of snapshots between the normal conformation and the primitive path.

BERs. This intrinsic mechanism of mechanical property modulation guides the versatile design of TINs, greatly broadening their applications in areas such as flexible electronics [47] and soft robotics [48,49]. Moreover, in some randomly cross-linked networks, molecular chain lengths also exhibit a geometric distribution, suggesting this regulation might be applicable in such systems [50,51].

Acknowledgments—X. X. acknowledges support from the Alexander von Humboldt-Stiftung. J. L. acknowledges the National Science Fund for Excellent Young Scholars (52122311) and the National Natural Science Foundation of China (52373222). This work was financially supported by the Academic Research Fund from the Singapore Ministry of Education (RG59/21 and MOE2019-T2-2-010) and the National Research Foundation, Singapore, under its 29th Competitive Research Program (CRP) Call (Grant No. NRF-CRP29-2022-0002).

[1] T. Maeda, H. Otsuka, and A. Takahara, Prog. Polym. Sci. **34**, 581 (2009).
[2] W. Zou, J. Dong, Y. Luo, Q. Zhao, and T. Xie, Adv. Mater. **29**, 1606100 (2017).
[3] B. V. Schmidt and C. Barner-Kowollik, Angew. Chem., Int. Ed. Engl. **56**, 8350 (2017).
[4] P. Chakma and D. Konkolewicz, Angew. Chem., Int. Ed. Engl. **58**, 9682 (2019).
[5] Z. Jiang, A. Bhaskaran, H. M. Aitken, I. C. Shackleford, and L. A. Connal, Macromol. Rapid Commun. **40**, 1900038 (2019).
[6] S. J. Rowan, S. J. Cantrill, G. R. Cousins, J. K. Sanders, and J. F. Stoddart, Angew. Chem., Int. Ed. Engl. **41**, 898 (2002).
[7] Y. Jin, C. Yu, R. J. Denman, and W. Zhang, Chem. Soc. Rev. **42**, 6634 (2013).
[8] R. J. Wojtecki, M. A. Meador, and S. J. Rowan, Nat. Mater. **10**, 14 (2011).
[9] C. Shao, H. Chang, M. Wang, F. Xu, and J. Yang, ACS Appl. Mater. Interfaces **9**, 28305 (2017).
[10] D. Li, P. Jing, L. Sun, Y. An, X. Shan, X. Lu, D. Zhou, D. Han, D. Shen, Y. Zhai *et al.*, Adv. Mater. **30**, 1705913 (2018).
[11] Q.-L. Lei, X. Xia, J. Yang, M. Pica Ciamarra, and R. Ni, Proc. Natl. Acad. Sci. U.S.A. **117**, 27111 (2020).
[12] T. F. Scott, A. D. Schneider, W. D. Cook, and C. N. Bowman, Science **308**, 1615 (2005).
[13] D. Montarnal, M. Capelot, F. Tournilhac, and L. Leibler, Science **334**, 965 (2011).
[14] S. Billiet, K. De Bruycker, F. Driessen, H. Goossens, V. Van Speybroeck, J. M. Winne, and F. E. Du Prez, Nat. Chem. **6**, 815 (2014).
[15] Z. Pei, Y. Yang, Q. Chen, E. M. Terentjev, Y. Wei, and Y. Ji, Nat. Mater. **13**, 36 (2014).
[16] B. Ghosh and M. W. Urban, Science **323**, 1458 (2009).
[17] G. Zhang, W. Peng, J. Wu, Q. Zhao, and T. Xie, Nat. Commun. **9**, 4002 (2018).
[18] B. Jin, H. Song, R. Jiang, J. Song, Q. Zhao, and T. Xie, Sci. Adv. **4**, eaao3865 (2018).
[19] D. J. Fortman, J. P. Brutman, C. J. Cramer, M. A. Hillmyer, and W. R. Dichtel, J. Am. Chem. Soc. **137**, 14019 (2015).
[20] X. Xia, P. Rao, J. Yang, M. P. Ciamarra, and R. Ni, JACS Au **2**, 2359 (2022).
[21] P. Taynton, K. Yu, R. K. Shoemaker, Y. Jin, H. J. Qi, and W. Zhang, Adv. Mater. **26**, 3938 (2014).
[22] O. R. Cromwell, J. Chung, and Z. Guan, J. Am. Chem. Soc. **137**, 6492 (2015).
[23] Z. P. Zhang, M. Z. Rong, and M. Q. Zhang, Adv. Funct. Mater. **28**, 1706050 (2018).
[24] K. Jin, L. Li, and J. M. Torkelson, Adv. Mater. **28**, 6746 (2016).
[25] H. Sun, C. P. Kabb, Y. Dai, M. R. Hill, I. Ghiviriga, A. P. Bapat, and B. S. Sumerlin, Nat. Chem. **9**, 817 (2017).
[26] W. Zou, B. Jin, Y. Wu, H. Song, Y. Luo, F. Huang, J. Qian, Q. Zhao, and T. Xie, Sci. Adv. **6**, eaaz2362 (2020).
[27] W. Miao, W. Zou, B. Jin, C. Ni, N. Zheng, Q. Zhao, and T. Xie, Nat. Commun. **11**, 4257 (2020).
[28] See Supplemental Material at http://link.aps.org/supplemental/10.1103/PhysRevLett.133.048101 for the simulation details and Fig. S1–S6.
[29] S. Plimpton, J. Comput. Phys. **117**, 1 (1995).
[30] C. Bennemann, W. Paul, J. Baschnagel, and K. Binder, J. Phys. Condens. Matter **11**, 2179 (1999).
[31] Q. Chen, Z. Zhang, Y. Huang, H. Zhao, Z. Chen, K. Gao, T. Yue, L. Zhang, and J. Liu, ACS Appl. Polym. Mater. **4**, 3575 (2022).
[32] Y. Fang, T. Yue, S. Li, Z. Zhang, J. Liu, and L. Zhang, Macromolecules **54**, 1095 (2021).
[33] J. R. Gissinger, B. D. Jensen, and K. E. Wise, Polymer **128**, 211 (2017).
[34] J. R. Gissinger, B. D. Jensen, and K. E. Wise, Macromolecules **53**, 9953 (2020).
[35] Z. Zhang, J. Liu, S. Li, K. Gao, V. Ganesan, and L. Zhang, Macromolecules **52**, 4154 (2019).
[36] B.-G. Xie, H. Wang, R.-L. Lu, H. Wang, R. Xia, P. Chen, and J.-S. Qian, Compos. Sci. Technol. **200**, 108398 (2020).
[37] D. Kroll and S. Croll, Polymer **79**, 82 (2015).
[38] J. Liu, Z. Zheng, F. Li, W. Lei, Y. Gao, Y. Wu, L. Zhang, and Z. L. Wang, Nano Energy **28**, 87 (2016).
[39] Q. Chen, W. Huang, P. Duan, T. Yue, L. Zhang, X. Wu, and J. Liu, Polymer **256**, 125233 (2022).
[40] J. Gao and J. Weiner, Macromolecules **24**, 1519 (1991).
[41] J. Gao and J. Weiner, J. Chem. Phys. **103**, 1614 (1995).
[42] R. Everaers, Eur. Phys. J. B Condens. Matter Complex Syst. **4**, 341 (1998).
[43] X. T. Ye, Macromolecules **38** (2005).
[44] R. Everaers, S. K. Sukumaran, G. S. Grest, C. Svaneborg, A. Sivasubramanian, and K. Kremer, Science **303**, 823 (2004).
[45] J. M. Ren, T. G. McKenzie, Q. Fu, E. H. Wong, J. Xu, Z. An, S. Shanmugam, T. P. Davis, C. Boyer, and G. G. Qiao, Chem. Rev. **116**, 6743 (2016).
[46] P. M. Claesson, R. Makuska, I. Varga, R. Meszaros, S. Titmuss, P. Linse, J. S. Pedersen, and C. Stubenrauch, Adv. Colloid Interface Sci. **155**, 50 (2010).
[47] J. Kang, D. Son, G.-J. Nathan Wang, Y. Liu, and J., Adv. Mater. **30**, 1706846 (2018).

[48] Y. Xia, G. Cedillo-Servin, R. D. Kamien, and S. Yang, Adv. Mater. **28**, 9637 (2016).
[49] Q. Xiaojie, C. Qiaomei, Y. Yang, X. Yanshuang, L. Zhen, W. Zhenhua, W. Yahe, W. Yen, and J. Yan, Adv. Mater. **30**, 1801103 (2018).
[50] N. Gnan, L. Rovigatti, M. Bergman, and E. Zaccarelli, Macromolecules **50**, 8777 (2017).
[51] V. Sorichetti, A. Ninarello, J. M. Ruiz-Franco, V. Hugouvieux, W. Kob, E. Zaccarelli, and L. Rovigatti, Macromolecules **54**, 3769 (2021).